



Monitoring of Gold Biodistribution from Nanoparticles Using a HPLC-Visible Method

Thomas Chaigneau, Arnaud Pallotta, Fatima Zahra Benaddi, Lucie Sancey,
Said Chakir, Ariane Boudier, Igor Clarot

► To cite this version:

Thomas Chaigneau, Arnaud Pallotta, Fatima Zahra Benaddi, Lucie Sancey, Said Chakir, et al.. Monitoring of Gold Biodistribution from Nanoparticles Using a HPLC-Visible Method. *Separations*, 2021, 8 (11), pp.215. 10.3390/separations8110215 . hal-03428709

HAL Id: hal-03428709

<https://hal.univ-lorraine.fr/hal-03428709>

Submitted on 15 Nov 2021

HAL is a multi-disciplinary open access archive for the deposit and dissemination of scientific research documents, whether they are published or not. The documents may come from teaching and research institutions in France or abroad, or from public or private research centers.

L'archive ouverte pluridisciplinaire **HAL**, est destinée au dépôt et à la diffusion de documents scientifiques de niveau recherche, publiés ou non, émanant des établissements d'enseignement et de recherche français ou étrangers, des laboratoires publics ou privés.



Distributed under a Creative Commons Attribution 4.0 International License

Article

Monitoring of Gold Biodistribution from Nanoparticles Using a HPLC-Visible Method

Thomas Chaigneau ¹, Arnaud Pallotta ^{1,2}, Fatima Zahra Benaddi ¹, Lucie Sancey ³, Said Chakir ⁴, Ariane Boudier ^{1,2} and Igor Clarot ^{1,2,*}

¹ Université de Lorraine, CITHEFOR, F-54000 Nancy, France; thomas.chaigneau@univ-lorraine.fr (T.C.); arnaud.pallotta@univ-lorraine.fr (A.P.); fatima.benaddi@univ-lorraine.fr (F.Z.B.); ariane.boudier@univ-lorraine.fr (A.B.)

² Nanocontrol, F-54000 Nancy, France

³ Centre de Recherche UGA/INSERM U1209/CNRS UMR5309, Institute for Advanced Biosciences, F-38700 La Tronche, France; lucie.sancey@univ-grenoble-alpes.fr

⁴ Environment and Health Laboratory, Faculty of Sciences, Moulay Ismail University, Zitoune, Meknes P.O. Box 11201, Morocco; saidchakire@gmail.com

* Correspondence: igor.clarot@univ-lorraine.fr



Citation: Chaigneau, T.; Pallotta, A.; Benaddi, F.Z.; Sancey, L.; Chakir, S.; Boudier, A.; Clarot, I. Monitoring of Gold Biodistribution from Nanoparticles Using a HPLC-Visible Method. *Separations* **2021**, *8*, 215. <https://doi.org/10.3390/separations8110215>

Academic Editor: Beatriz Albero

Received: 30 September 2021

Accepted: 10 November 2021

Published: 12 November 2021

Publisher's Note: MDPI stays neutral with regard to jurisdictional claims in published maps and institutional affiliations.



Copyright: © 2021 by the authors. Licensee MDPI, Basel, Switzerland. This article is an open access article distributed under the terms and conditions of the Creative Commons Attribution (CC BY) license (<https://creativecommons.org/licenses/by/4.0/>).

1. Introduction

Nanoparticles (NPs) are widely used in many fields, particularly the biomedical field. Among them, gold nanoparticles (AuNPs) are well described for their functionalization with active substances to serve as a drug reservoir [1,2] or in the context of cancer diagnostics or treatment [3–6]. They are also studied for their antibacterial properties [7,8]. The intensive development of therapies or imaging techniques using gold nanoparticles has raised the question of the fate of the corresponding NPs, as well as the metal at various redox states originating from them in organisms. The knowledge of the biodistribution and the pharmacokinetics of NPs and their by-products (aggregates of nanoparticles, metal ions, etc.), is crucial for the development of the new candidate in nanomedicine. The nanoparticle distribution is closely linked to the route of administration [9], as well as their biophysical properties, including size, surface charge, and aggregation state [10]. These different elements lead to an increased complexity in evaluating the fate of these nanoobjects [11]. Imaging techniques that monitor the distribution and potential accumulation of NPs are important, but analytical methods are necessary and complementary to obtain the distribution profile of NPs and NP degradation products in organs and tissues [12]. This major question refers to the development of analytical methods to quantify gold in various biological matrices. The reference method for the determination of gold is ICP-MS (inductively coupled plasma-mass spectrometry) [13]. However, such direct quantification

leads to problematic gold recoveries in biological media [14], sometimes associated with difficulties in accessibility. To overcome these problems, a large number of alternative methods have been developed, and the most commonly used are described in Table 1.

Table 1. Analytical methods for gold quantification in biological samples.

Method	Matrix	Advantages/Drawbacks	Ref.
ICP-MS	Aqueous	LOQ: 0.15 µg/L (in Au ³⁺) Matrix-dependent Low recovery ratios (<50%)	[14]
ICP-MS	Rat tissues and organs	Long preparation time High amount of tissue required (>0.3 g) Matrix-dependent Recovery issues (from 90–135%)	[15]
LA-ICP-MS	Rice	Only usable under controlled conditions (specific matrix composition, element, etc.)	[16]
spICP-MS	Nematode	NP number measurement Size and distribution information Matrix-dependent	[17]
Total reflection X-ray fluorescence	Human tumor cells	Time-dependent recovery Matrix-dependent	[18]
INAA	Mice tissues and organs	Complex apparatus Long preparation time Radioactive samples	[19]
GF-AAS	Beef liver, kidneys, and bones	LOQ: 1.0 ng/g of tissues High amount of tissue required (>1.0 g)	[20]
ET-AAS	Human hair sample	High amount of tissue required (>0.5 g) Matrix-dependent Not specific to gold	[21]

ET-AAS: Electrothermal atomic absorption spectrometry; GF-AAS: Graphite furnace atomic absorption spectrophotometry; ICP-MS: Inductively coupled plasma-mass spectroscopy; INAA: Instrumental neutron activation analysis; LA-ICP-MS: Laser ablation-inductively coupled plasma-mass spectroscopy; spICP-MS: Single-particle inductively coupled plasma mass spectrometry; LOQ: Limit of quantification.

Without taking into consideration the availability and the price of the apparatus mentioned in Table 1, direct or indirect determinations of gold by most of these methods induce analytical issues due to the interferences between biological components or method sensitivity. Treatment steps parallel to the analyte concentration in the sample are required to ensure the repeatability and reproducibility of results and to reach the needed limit of quantification (LOQ). However, they often lead to a lack of recovery and also are matrix-dependent. Recoveries in ICP-MS are directly influenced not only by acidic/basic conditions and salt concentrations, but also by the size distribution of AuNPs [14,15].

In a previous work, we developed and optimized a HPLC-vis method to quantify Au³⁺ from AuNPs in buffer using liquid–liquid extraction of an gold–rhodamine B ion pair in diisopropylether [22]. Although we achieved this optimization in terms of the limit of detection (LOD; 0.1 µM of Au³⁺), the quantification in complex matrices (blood plasma, cells, tissues, etc.) remains very challenging. As stated before, complex matrices contain many analytes able to interfere with treatment: Blood proteins can stack at the interface between water and organic solvent, avoiding the ion pair being extracted; rhodamine B can interact with many components of the matrix; and the use of acidic digestion

(trifluoroacetic acid, aqua regia, etc.) can lead to unfavorable conditions to form the ion pair. Thus, although this method is efficient in simple aqueous media, it shows numerous drawbacks against biological matrices such as blood plasma, cells, or tissues. We sought to overcome these issues through the addition of a carbonization step prior to extraction. The method was developed with organs/plasma spiked with an AuNP suspension, then used to quantify gold *in vivo* in mice at different times after intravenous injection of 5 nm of citrate AuNPs.

The aim of this paper was to validate the newly developed method on different mouse/rat organs in terms of the lower limit of quantification, linearity, recovery and accuracy to finally quantify gold from AuNPs in the different organs. We also provide a preliminary overview of the AuNP biodistribution after IV injection that can be compared to profiles found in the literature.

2. Materials and Methods

2.1. Chemicals

A phosphate-buffered saline (PBS) solution was prepared as follows: $[\text{Na}_2\text{HPO}_4] = 6.48 \times 10^{-3}$ M, $[\text{KH}_2\text{PO}_4] = 1.47 \times 10^{-3}$ M, $[\text{NaCl}] = 138.00 \times 10^{-3}$ M, and $[\text{KCl}] = 2.68 \times 10^{-3}$ M, with the final pH adjusted to 7.4. All other reagents were supplied by Sigma Aldrich (St. Louis, MO, USA) and were of analytical grade. Ultrapure deionized water ($>18.2 \text{ M}\Omega\text{.cm}$) was used for the preparation of all solutions.

2.2. Biological Tissues and Fluids

All experiments were performed in accordance with the European Community guidelines (2010/63/EU) for the use of experimental animals. Protocols and procedures were approved by the regional and national ethical committees on animal experiments (no. APAFIS#15598-2018061619129620v3 for rats and APAFIS#9363 for mice).

Organs from male Wistar rats between 280 and 350 g and C57Bl6 mice (Charles River, France) were used in this study. Organs and blood were collected right after euthanasia. The blood was obtained directly from an artery through a short PTFE catheter (Intraflon 2, Vygon, Écouen, France) and collected in Vacutainer (Becton Dickinson, Franklin Lakes, NJ, USA) tubes containing heparin lithium. Plasma was obtained after centrifugation ($10,000 \times g$, 15 min, 4°C) and keep at -20°C .

A colloidal AuNP suspension was injected into the mice (NMRI, Janvier Labs, Le Genest-Saint-Isle, France) according to the following protocol: 200 μL of AuNP suspension injected intravenously (IV) into 6 mice, corresponding to an injected dose (ID) of 38 nmol of Au^{3+} . Three mice were euthanized after 30 min, and the other 3 after 1 h. Organs were removed and frozen (-80°C) before analysis. To track the AuNP distribution, urine was also collected within the bladder (30 and 60 min after injection) and analyzed.

As the suspension was injected into the bloodstream, the organs selected as priority were those classically described in the literature: The liver, kidneys, and spleen [23]. For a more complete validation of our method, we added the brain, because some authors have suggested that small-sized NPs ($<10 \text{ nm}$) can accumulate there, as well as the lungs, which are well known in exposure to nanoparticles by inhalation.

2.3. AuNP Synthesis

Citrate-stabilized gold nanoparticles were synthesized in the lab according to [24]. Briefly, a gold salt solution (AuCl_4^-) was added into 90 mL of ultrapure water, giving a final concentration of 270 μM , and 2 mL of sodium citrate (55 mM) was added under an inert atmosphere. The solution was stirred for 1 min and 1.0 mL of NaBH_4 (19.5 mM) was added, following which the solution was stirred for another 5 min. The final concentration of gold nanoparticles was 90 nM, equivalent to 270 μM of Au^{3+} according to [22]. The resulting suspension was immediately stored in the dark at 4°C for a maximum of 20 days, as described in [25]. The AuNPs obtained were completely described in terms of plasmonic resonance band, hydrodynamic diameter, charge, and purity, as evaluated in [26], and their

gold core diameter was measured at 5.3 ± 1.1 nm. See Supplementary Materials Section S1 for more information on the characterization of the synthesized batches used in this study.

2.4. Au^{3+} Quantification

2.4.1. Sample Treatment

Sample preparation was adapted with modifications from a previous work developed in simple matrices [22]. Crucibles (VWR, 459-1601) were first rinsed with HCl-NaCl-Br₂ solution (15 min, 800 μL , 1.0 M–0.3 M–0.025 M, respectively) and burnt in a muffle furnace (Nabertherm LE2/11, Nabertherm GmbH, Lilienthal, Germany) at 900 °C for 1 h before use. The biological matrices (organs or fluids) were then weighed in the crucible (spiked with AuNPs or not) and a simple 60 min carbonization step under air (atmospheric pressure) at 900 °C in a muffle furnace was set up. After cooling down to room temperature, the crucibles were rinsed with a HCl-NaCl-Br₂ solution (15 min, 800 μL , 1.0 M–0.3 M–0.025 M, respectively) under slight agitation. Then, 400 μL of the resulting solution was mixed with 400 μL of PBS in LoBind Eppendorf microtubes (1.5 mL). The mixture was then partially evaporated using a Turbovap (Biotage, Uppsala, Sweden) at 40 °C under inert gas (N₂, 4 psi) for 15 min to eliminate traces of Br₂ that could react with rhodamine B (Rho B). Next, 200 μL of NH₄Cl solution (30% *m/V*), 100 μL of 6 M HCl, and 100 μL of rhodamine B solution (0.084 μM) were finally added. For the extraction of the ion pair formed between tetrachloroaurate anion and rhodamine B, 300 μL of diisopropyl ether was added. The microtubes were agitated on a Vibramax 100 (Heidolf Instruments) for 3 min at 1500 rpm, then centrifuged (Mini Spin Plus, Eppendorf, Hambourg, Germany) for 30 s at 14,100 $\times g$. Following this, 150 μL of the supernatant (organic phase) was withdrawn, dried and evaporated (Turbovap, 5 min, N₂ 4 psi), and the residue was dissolved in a mobile phase (150 μL) before injection into the HPLC system (Prominence, Shimadzu, Columbia, MD, USA). Particular attention was required to prevent any risk of toxicity and injury during NP synthesis and oxidation (specific protective gloves, glasses, and fume hood).

2.4.2. HPLC Quantification

HPLC analysis was performed on a Shimadzu system (Prominence, Shimadzu, Columbia, MD, USA) constituted by the following modules: Degasser, quaternary pump (LC 20AD), autosampler (SIL 20AC), oven, and UV-Visible detector (SPD20A, Shimadzu, Columbia, MD, USA). The column (Nucleosil® C18 Macherey-Nagel 150 mm × 4.6 mm, 3 μm particle size 100 Å) was thermostated at 40 °C. The mobile phase consisted of a mixture of acetonitrile and 0.1% trifluoroacetic acid aqueous solution (25/75, *V/V*). The injection volume was 100 μL (with the help of a 200 μL insert placed in the injector vial). The detector was set at 555 nm, and the pump at a flow rate of 1.0 mL min^{-1} . Data acquisition was performed using Shimadzu LabSolution.

The Au^{3+} quantities found in the crucibles were determined from the calibration curves obtained using 400 μL of gold salt AuCl_4^- solution in the range of 1.0–20.0 μM in PBS mixed with 400 μL of HCl-NaCl-Br₂ in LoBind Eppendorf microtubes (1.5 mL) that were treated as described above [22]. The obtained concentration corresponded to 0.8–16 nmol of Au^{3+} in the crucibles.

The standards in complex matrices used for the validation steps were: Specificity, linearity, quantification limit, precision, and recovery. These were prepared as follows: 100 μL of 5 different dilutions in PBS of AuNP suspension were added into a crucible with an appropriate quantity of organs (50–500 mg) before carbonization in a muffle furnace. For the blank samples used to assess specificity, biological matrices were replaced by 100 μL of PBS. The quantity of Au^{3+} added was controlled by quantifying Au^{3+} in the AuNP suspension treated with HCl-NaCl-Br₂ solution before dilution in PBS and spiking in the crucible.

2.5. Method Validation

The method was validated according to the ICH guidelines [27] and FDA recommendations [28].

3. Results and Discussion

3.1. Preliminary Study

The first steps of development involved the use of a previously described method [22] with slight modifications. Gold (Au^{3+}) and blank samples were analyzed in the presence or absence of liver to highlight an eventual matrix effect. Briefly, 10 mg of rat liver were digested in 400 μL of hydrochloric acid (12 M) in an ultrasonic bath until full dissolution (homogeneous suspension), followed by the addition of $\text{NaCl}-\text{Br}_2$ solution (400 μL , 0.3 M–0.025 M, respectively) (see Supplementary Materials Section S2 for more information on the experimental conditions used in this preliminary study). The ion pair of Rho B– AuCl_4^- was then quantified as described. The results are shown in Figure 1.

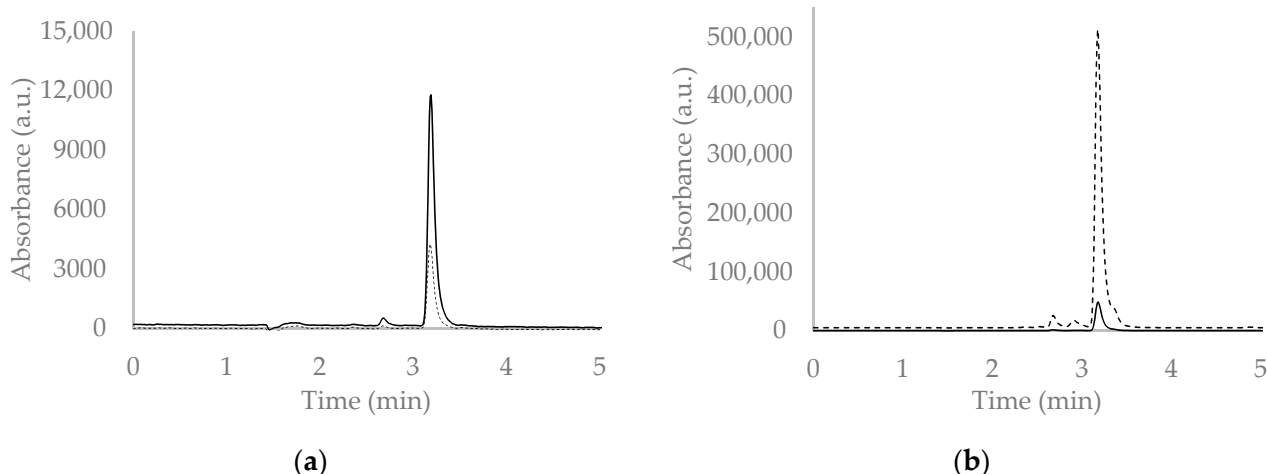


Figure 1. Chromatograms of (a) 0.0 μM of AuCl_4^- and (b) 10.0 μM of AuCl_4^- in presence (plain line) or absence (dashed line) of rat liver.

The blank sample chromatograms presented higher interferences with Rho B in the presence of liver compared to a simple matrix such as PBS (Figure 1a). Moreover, the matrix effect was even more important when gold salt was added to the samples. The signal corresponding to the Rho B– AuCl_4^- ion pair was decreased by a ten-fold factor between PBS and the liver matrix (Figure 1b). This could indicate that the ion pair was prevented from forming or that the extraction yield was lessened. It was hypothesized that the matrix (proteins, fatty acids, lipids, etc.) interfered with the ion pair formation or extraction mechanism. In any case, this led to a dramatic rise in the limit of detection (LOD).

To overcome these issues, different sample treatments such as protein precipitation (with organic or acidic conditions), sample centrifugation, and modification of acidic digestion (aqua regia) were considered without success.

Finally, to avoid the matrix effect, a carbonization (dry ashing) step was developed.

3.2. Carbonization Step Optimization

Three parameters were optimized—temperature, duration, and biological sample quantity (from rat). The aim was to obtain the least possible ashes remaining in the crucible, indicating a complete combustion of the sample, so after different temperatures were tested (600, 800, and 900 $^\circ\text{C}$), the oven was finally set to 900 $^\circ\text{C}$, far over the classical carbonization temperature [29]. Three carbonization times were tested—30, 60, and 90 min. After 30 min at 900 $^\circ\text{C}$, the combustion was not complete. No significant difference between 60 and 90

min was observed, as no ash remained in the crucibles. The condition, 1 h at 900 °C, was selected for sample treatment. Once these parameters were set, the impact of the tissue quantity was finally assessed. Several masses of rat liver (from 0 (control) to 1000 mg) were deposited in the crucible, spiked by the addition of 10 µL of the standard AuNP suspension (270 µM Au³⁺) corresponding to the addition of 2.7 nmol of Au³⁺. The results of the HPLC quantification are shown in Figure 2.

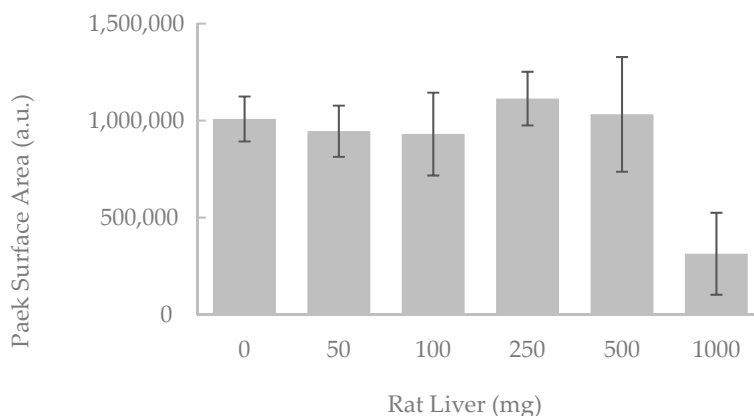


Figure 2. Chromatographic peak surface area (mean \pm standard deviation) from an addition of 10 µL of AuNP suspension (2.7 nmol Au³⁺ added) in crucibles containing different rat liver masses ($N = 3$).

The detector response was similar up to 500 mg of liver. For validation, 250 mg of liver or 100 µL of plasma were selected (from rats). It is interesting to note that the method was also adapted for low-mass tissues from 50 to 100 mg, crucial for small organs such as the spleen or kidneys, which are of great importance in biodistribution studies of NPs. To reduce the standard deviation in the method validation step, it was also chosen to use a bigger spike volume of 100 µL.

3.3. Method Validation

The method was validated according to the ICH guidelines [27] and FDA recommendations [28] for AuNPs in Wistar rat plasma and liver. As the preliminary results obtained (pre-validation) on the rat and mice organs were very similar, the method validation was only realized using rat organs. The validation criteria considered are described in the following paragraphs.

3.3.1. Specificity

Specificity was assessed by analyzing PBS samples, blanks (no AuNPs), or spiked (100 µL of AuNP suspension) liver or plasma samples, from at least six different rats. No interfering peak was observed in the chromatograms, proving the method specificity.

3.3.2. Linearity and Quantification Limits

The linearity was evaluated for calibration curves using standards in two biological matrices (rat liver and plasma). The AuNP suspension was diluted and spiked (100 µL) to obtain a calibration range from 1.0 to 10.6 nmol of Au³⁺ in 100 µL of plasma and from 1.0 to 14.6 nmol of Au³⁺ added to 250 mg of rat liver, leading to concentrations of 10.6–106.5 nmol/mL in the plasma and 3.9–58.5 nmol/g in the liver. Standards were treated as described in Section 2.4. Typical chromatograms are shown in Figure 3 and the results are summarized in Table 2.

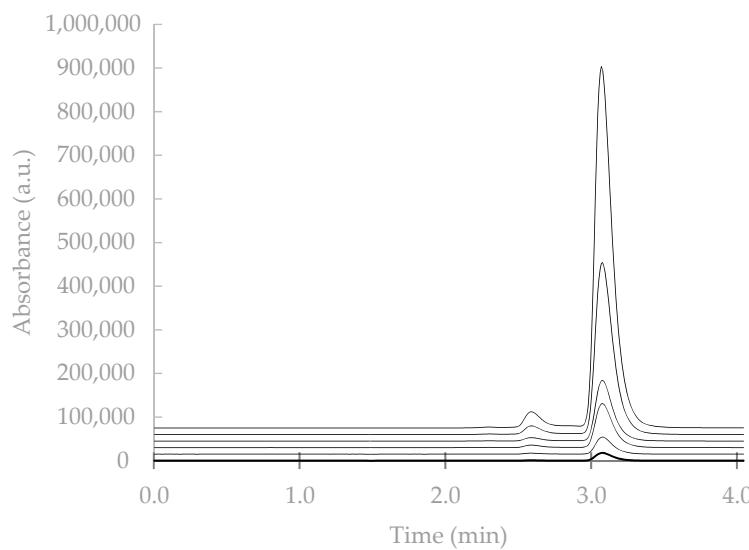


Figure 3. Typical HPLC chromatograms of blank (bold solid line, spiked with 100 μL of PBS without Au^{3+}) and five Au^{3+} quantities (plain lines, corresponding to 1.0, 2.2, 4.0, 8.0, and 10.6 nmol, from the smallest to the largest peak, respectively, obtained after spiking 100 μL of AuNP suspension on 250 mg rat liver.

Table 2. Statistical evaluation (*F*-test) of linearity for the Au^{3+} quantity from AuNPs added to 100 μL of rat plasma or added to 250 mg of rat liver (five quantities on three days) with a linear regression model.

Linear Model	Definition	<i>F</i> Theoretical Value	Plasma	Liver
Range (nmol of Au^{3+})			[1.1–10.6]	[1.0–14.6]
Slope \pm SD			$587,292 \pm 46,288$	$519,240 \pm 34,778$
Intercept \pm SD			$-826,551 \pm 291,771$	$-330,827 \pm 262,971$
Correlation Coeff (<i>R</i>)			0.989	0.993
<i>F</i> regression	<i>F</i> -value 0.01	10.04	1564.85	1723.22
<i>F</i> lack of fit	<i>F</i> -value 0.01	6.55	5.70	3.85

SD: Standard deviation.

Statistical evaluation (classical *F*-test) of the data showed that linear regression was a suitable model to quantify gold from AuNPs in rat plasma and liver. However, a Student's *t*-test performed on slopes and intercepts showed a significant difference between the plasma and liver models (at risk $\alpha = 5\%$). These results indicate the necessity to perform calibration using standards prepared in the studied biological matrix to quantify AuNPs.

The lower limits of quantification (LLOQs), defined as the lowest calibration points with a relative standard deviation (RSD) below 20%, were set to be the lowest points of calibration curves (i.e., 1.0 nmol of Au^{3+} or 10.6 nmol/mL in plasma and 1.1 nmol of Au^{3+} or 3.9 nmol/g in the liver).

3.3.3. Precision and Recovery

Precision was expressed by the RSD of the recovered gold on three different days for three different concentrations of calibration curves. The recovery rate (RR) was evaluated by calculating the ratio between the gold quantity added and the gold quantity recovered. The exact quantity added was determined using a gold salt standard calibration curve. The quantity found in the crucible after carbonization was determined using the same calibration curve. The results are shown in Table 3.

Table 3. Au³⁺ recovery and repeatability obtained after the addition of various quantities of Au³⁺ issued from diluted AuNP suspensions in 100 µL of rat plasma or added to 250 mg of rat liver ($N = 3$).

Matrix	Added	Recovered	RR (%)	RSD (%)
	nmol eq. Au ³⁺	nmol eq. Au ³⁺ (\pm SD)		
Plasma	1.1	0.7 \pm 0.1	62.1%	7.9%
	8.0	7.2 \pm 0.6	89.5%	6.3%
	10.6	10.2 \pm 0.6	95.4%	6.3%
Liver	1.0	0.9 \pm 0.1	91.2%	5.5%
	7.3	6.0 \pm 0.5	81.7%	8.1%
	14.6	11.2 \pm 0.2	76.5%	1.9%

RR: Recovery rate; SD: Standard deviation; RSD: Relative standard deviation.

The recoveries were calculated on low, middle, and high quantities added from the calibration curves. The experiments were realized on the livers and plasma from different rats with an RSD below 10%, indicating high repeatability of the results. Calculated recoveries were satisfactory, with an overall yield of $82 \pm 12\%$. For the plasma, the lowest recovery rate was found for the lowest calibration point (1.1 nmol). On the contrary, in the liver, the highest recovery rate was found for the same point (1.0 nmol). This showed that more complex matrices have a higher impact on gold recovered at low concentrations (greater matrix effect), leading to overestimation of the recovery rate near the LOQ. Gold recovery was assessed on matrix-free crucibles (no plasma or liver). The resulting RR was found to be $84 \pm 6\%$, indicating that recovery loss was not only linked to the matrix effect, but could also be explained by the sample treatment.

It appeared that the matrices played a key role in the method validation, implying the necessity to have an individual calibration curve for each biological matrix targeted (fluids and organs from each species).

3.4. Application of AuNPs in Various Tissues

The RR was calculated in other rat organs (kidneys, lungs, and spleen) and mouse organs (kidneys, lungs, spleen, brain, and urine). The results were compared with data obtained from rat liver validation.

3.4.1. Recovery Rates in Other Rat Organs

Kidneys, lungs, and spleens were selected as targeted organs, as they are known to be able to stock AuNPs after inhalation or injection [11]. Approximately 250 mg of organs were exposed to 5 nm of AuNPs (spiked with approximately 8 nmol eq. Au³⁺) and evaluated with the previously developed method for gold quantification. The results of RR and RSD are shown in Table 4.

Table 4. Gold RR and repeatability obtained in other rat organs.

Matrix	Added	Recovered	RR (%)	RSD (%)
	nmol eq. Au ³⁺	nmol eq. Au ³⁺ (\pm SD)		
Kidneys	7.3	6.2 \pm 0.3	85.0%	4.1%
Lungs	8.9	6.7 \pm 0.2	74.9%	3.4%
Spleen	7.7	6.6 \pm 0.5	85.9%	7.9%

RR: Recovery rate; SD: Standard deviation; RSD: Relative standard deviation.

All gold quantities recovered were included in the rat liver RR dispersion (i.e., $81.7 \pm 8.1\%$) obtained in the validation study (Section 3.3.3). These quality controls (QCs) indicated that while a calibration curve was required for each organ, the complete validation of the model may not be necessary to quantify gold in other rat organs.

3.4.2. AuNPs in Mice Samples

To ensure the applicability of our method to other species, several calibration curves in various C57Bl6 mouse tissues were realized (same ranges as previously described). The RR was calculated using the ratio between the slopes of the mouse calibration curves and the gold salt calibration curve. The results are shown in Table 5.

Table 5. AuNP linearity and recovery in mice organs.

Matrix	Slope \pm SD	Intercept \pm SD	Correlation Coefficient (<i>R</i>)	RR %
Plasma	620,066 \pm 41,726	-666,135 \pm 171,636	0.991	90.4
Liver	608,729 \pm 25,900	-207,410 \pm 141,706	0.995	83.4
Kidneys	623,413 \pm 31,670	-654,325 \pm 191,653	0.992	91.9
Spleen	461,238 \pm 73,935	-667,931 \pm 438,089	0.928	76.6
Brain	319,917 \pm 15,421	-184,616 \pm 95,505	0.993	66.3
Urine	497,046 \pm 37,805	-652,743 \pm 195,491	0.983	100.7

SD: Standard deviation.

The regression equations presented satisfactory correlation coefficients ranging between 0.928 in the spleen to 0.995 in the liver, indicating that the linear model was also adapted to quantify gold in other organs or fluids from mice. All organs presented an RR between 80% and 100%, except for the brain, showing a 66% recovery. This difference could be explained by the greater amount of brain tissue used for calibration (approximately 500 mg, corresponding to the entire brain) or the very different nature of this organ compared to those already tested (containing more fat). In this case, a longer carbonization time may be necessary. All of these assays showed the robustness of the method in terms of organ and species.

3.5. Application: *In Vivo* Gold Quantification from AuNP Distribution after IV Injection

Organs and fluids from AuNP-exposed mice were analyzed with the validated method, and gold distribution was assessed. Quantified gold was expressed as the quantity of Au^{3+} (nmol) in each organ and the percentage of the injected dose (% ID): 38 nmol Au^{3+} . The concentration in each organ (nmol/g of tissue) or fluid (nmol/L) was also calculated. The results are shown in Table 6.

Table 6. Gold quantification and concentration in mice tissues and fluid after 30 min and 1 h.

Matrix	30 min		60 min	
	Au^{3+} (nmol) (% ID)	Au^{3+} per Organ Mass (nmol/g) or Fluid Volume (nmol/mL)	Au^{3+} (nmol) (% ID)	Au^{3+} per Organ Mass (nmol/g) or Fluid Volume (nmol/mL)
Plasma	<LLOQ	<LLOQ	<LLOQ	<LLOQ
Liver	6.5 \pm 1.9 (17.1%)	33.0 \pm 7.4	11.1 \pm 1.5 (29.1%)	41.3 \pm 5.7
Kidneys	1.5 \pm 0.1 (3.8%)	7.8 \pm 1.9	1.4 \pm 0.1 (3.6%)	7.5 \pm 2.1
Spleen	3.2 \pm 0.2 (8.4%)	53.4 \pm 39.3	3.4 \pm 0.1 (9.0%)	84.1 \pm 43.9
Brain	<LLOQ	<LLOQ	<LLOQ	<LLOQ
Urine	<LLOQ	<LLOQ	<LLOQ	<LLOQ

<LLOQ: Below the lower limit of quantification; uncertainties evaluated by the corresponding standard deviations.

After IV injection, AuNPs were directly distributed in the organism and were able to freely diffuse to other organs. Higher concentrations were observed in the spleen, followed by the liver and kidneys. In the kidneys and spleen, the results were similar at both times, but in the liver, gold accumulation was ongoing up to 60 min. This distribution showed that the uptake of AuNPs was primarily linked to the mononuclear phagocyte system mainly found in the liver, spleen, and kidneys. Circulating AuNPs were captured by this system to be removed by the organism. This can also explain why AuNPs were not found in the plasma after 30 min of exposition. The AuNP concentration in the plasma may have

already been too low. Analyzing larger plasma quantities or setting a shorter sampling time could be a solution. It appears that no AuNPs were found in the brain, indicating an absence of the blood–brain barrier (BBB) crossing, or at very few concentrations both times. Sonavane et al. [30] already reported a study about AuNP biodistribution, where he stated that 15 nm of AuNPs is able to cross the BBB thanks to their small size. However, it is important to note that the concentrations used in that study were 20,000 times higher than that used in the present paper, and the %ID found in the brain was 0.075%. In our study, this represents an Au quantity of 0.03 nmol, far below any LOQ method. The BBB crossing might be explained by a tissue impregnation that did not occur in the present paper. The other results are consistent with the literature [31,32], as the highest gold concentration was found in the spleen. Finally, urine was analyzed to assess whether gold was excreted through the kidneys or not. The results were all below the LLOQ, meaning that the collection time began too late or that the AuNPs were excreted via another route, such as in feces. In any case, only 42% of the injected dose was found after quantification. This raises several questions in terms of target organs, collection time, gold dissemination, LLOQ, etc. Compared to other studies, the quantity of injected AuNPs was less important, but may be more representative of a real exposition to AuNPs [33].

4. Conclusions

In this paper, we developed a sample treatment method to limit the biological matrix effect. High-temperature carbonization proved to be an efficient way to allow HPLC/Vis quantification of gold from AuNPs, with little impact from the matrix (organs or animal species). After a complete validation according to the ICH and/or FDA recommendations, this method was used to quantify gold in mice after IV injection. The results showed an accumulation of gold mainly in liver, spleen, and kidneys, with none or under the LLOQ in urine excretion. Our results show that a simple HPLC/Vis method is perfectly useful for evaluating the biodistribution of gold from NP injection and specifically, as we have discussed, with injections of low AuNP doses compared to the literature and probably more representative of the quantities expected by real exposure.

Supplementary Materials: The following are available online at <https://www.mdpi.com/article/10.3390/separations8110215/s1>, Section S1: AuNP characterization; Figure S1: TEM analyzes on AuNP-Citrate; Section S2: Preliminary study.

Author Contributions: Conceptualization, I.C. and A.B.; methodology, I.C.; validation, T.C. and A.P.; resources, T.C., A.P., F.Z.B., L.S. and S.C.; writing—original draft preparation, T.C. and A.P.; writing—review and editing, T.C., A.P., A.B. and I.C.; supervision, A.B. and I.C. All authors have read and agreed to the published version of the manuscript.

Funding: This research received no external funding.

Institutional Review Board Statement: The study was conducted according to the guidelines of the Declaration of Helsinki, and performed in accordance with the European Community guidelines (2010/63/EU) for the use of experimental animals. Protocols and procedures were approved by the regional and national ethical committees on animal experiments (no. APAFIS#15598-2018061619129620v3 for rats and APAFIS#9363 for mice).

Acknowledgments: The authors would like to thank UMR 1256 NGERE for providing the mouse organs and fluids used for calibration and François Dupuis for providing the rat plasma.

Conflicts of Interest: The authors declare no conflict of interest.

References

1. Ghosh, P.; Han, G.; De, M.; Kim, C.K.; Rotello, V.M. Gold Nanoparticles in Delivery Applications. *Adv. Drug Deliv. Rev.* **2008**, *60*, 1307–1315. [[CrossRef](#)] [[PubMed](#)]
2. Kong, F.-Y.; Zhang, J.-W.; Li, R.-F.; Wang, Z.-X.; Wang, W.-J.; Wang, W. Unique Roles of Gold Nanoparticles in Drug Delivery, Targeting and Imaging Applications. *Molecules* **2017**, *22*, 1445. [[CrossRef](#)]
3. Boisselier, E.; Astruc, D. Gold Nanoparticles in Nanomedicine: Preparations, Imaging, Diagnostics, Therapies and Toxicity. *Chem. Soc. Rev.* **2009**, *38*, 1759–1782. [[CrossRef](#)]

4. Sztandera, K.; Gorzkiewicz, M.; Klajnert-Maculewicz, B. Gold Nanoparticles in Cancer Treatment. *Mol. Pharm.* **2019**, *16*, 1–23. [[CrossRef](#)] [[PubMed](#)]
5. Gerosa, C.; Crisponi, G.; Nurchi, V.M.; Saba, L.; Cappai, R.; Cau, F.; Faa, G.; Van Eyken, P.; Scartozzi, M.; Floris, G.; et al. Gold Nanoparticles: A New Golden Era in Oncology? *Pharmaceutics* **2020**, *13*, 192. [[CrossRef](#)] [[PubMed](#)]
6. Zhang, A.; Nakanishi, J. Improved Anti-Cancer Effect of Epidermal Growth Factor-Gold Nanoparticle Conjugates by Protein Orientation through Site-Specific Mutagenesis. *Sci. Technol. Adv. Mater.* **2021**, *22*, 616–626. [[CrossRef](#)]
7. Zhao, Y.; Tian, Y.; Cui, Y.; Liu, W.; Ma, W.; Jiang, X. Small Molecule-Capped Gold Nanoparticles as Potent Antibacterial Agents That Target Gram-Negative Bacteria. *J. Am. Chem. Soc.* **2010**, *132*, 12349–12356. [[CrossRef](#)] [[PubMed](#)]
8. Gouyau, J.; Duval, R.E.; Boudier, A.; Lamouroux, E. Investigation of Nanoparticle Metallic Core Antibacterial Activity: Gold and Silver Nanoparticles against Escherichia Coli and Staphylococcus Aureus. *Int. J. Mol. Sci.* **2021**, *22*, 1905. [[CrossRef](#)]
9. Missaoui, W.N.; Arnold, R.D.; Cummings, B.S. Toxicological Status of Nanoparticles: What We Know and What We Don't Know. *Chem. Biol. Interact.* **2018**, *295*, 1–12. [[CrossRef](#)]
10. Wu, T.; Tang, M. Review of the Effects of Manufactured Nanoparticles on Mammalian Target Organs. *J. Appl. Toxicol.* **2018**, *38*, 25–40. [[CrossRef](#)]
11. Najahi-Missaoui, W.; Arnold, R.D.; Cummings, B.S. Safe Nanoparticles: Are We There Yet? *Int. J. Mol. Sci.* **2021**, *22*, 385. [[CrossRef](#)] [[PubMed](#)]
12. Arms, L.; Smith, D.W.; Flynn, J.; Palmer, W.; Martin, A.; Woldu, A.; Hua, S. Advantages and Limitations of Current Techniques for Analyzing the Biodistribution of Nanoparticles. *Front. Pharmacol.* **2018**, *9*, 802. [[CrossRef](#)]
13. Scheffer, A.; Engelhard, C.; Sperling, M.; Buscher, W. ICP-MS as a New Tool for the Determination of Gold Nanoparticles in Bioanalytical Applications. *Anal. Bioanal. Chem.* **2008**, *390*, 249–252. [[CrossRef](#)] [[PubMed](#)]
14. Allabashi, R.; Stach, W.; de la Escosura-Muñiz, A.; Liste-Calleja, L.; Merkoçi, A. ICP-MS: A Powerful Technique for Quantitative Determination of Gold Nanoparticles without Previous Dissolving. *J. Nanopart. Res.* **2008**, *11*, 2003. [[CrossRef](#)]
15. De Jong, W.H.; Hagens, W.I.; Krystek, P.; Burger, M.C.; Sips, A.J.A.M.; Geertsma, R.E. Particle Size-Dependent Organ Distribution of Gold Nanoparticles after Intravenous Administration. *Biomaterials* **2008**, *29*, 1912–1919. [[CrossRef](#)]
16. Koelmel, J.; Leland, T.; Wang, H.; Amarasiriwardena, D.; Xing, B. Investigation of Gold Nanoparticles Uptake and Their Tissue Level Distribution in Rice Plants by Laser Ablation-Inductively Coupled-Mass Spectrometry. *Environ. Pollut.* **2013**, *174*, 222–228. [[CrossRef](#)]
17. Johnson, M.E.; Hanna, S.K.; Montoro Bustos, A.R.; Sims, C.M.; Elliott, L.C.C.; Lingayat, A.; Johnston, A.C.; Nikoobakht, B.; Elliott, J.T.; Holbrook, R.D.; et al. Separation, Sizing, and Quantitation of Engineered Nanoparticles in an Organism Model Using Inductively Coupled Plasma Mass Spectrometry and Image Analysis. *ACS Nano* **2017**, *11*, 526–540. [[CrossRef](#)]
18. Mankovskii, G.; Pejović-Milić, A. Comparison of Total Reflection X-Ray Fluorescence Spectroscopy and Inductively Coupled Plasma Atomic Emission Spectroscopy for Thequantification of Gold Nanoparticle Uptake. *Spectrochim. Acta Part B At. Spectrosc.* **2020**, *164*, 105764. [[CrossRef](#)]
19. Hillyer, J.F.; Albrecht, R.M. Correlative Instrumental Neutron Activation Analysis, Light Microscopy, Transmission Electron Microscopy, and X-Ray Microanalysis for Qualitative and Quantitative Detection of Colloidal Gold Spheres in Biological Specimens. *Microsc. Microanal.* **1998**, *4*, 481–490. [[CrossRef](#)] [[PubMed](#)]
20. Kehoe, D.F.; Sullivan, D.M.; Smith, R.L. Determination of Gold in Animal Tissue by Graphite Furnace Atomic Absorption Spectrophotometry. *J. AOAC Int.* **1988**, *71*, 1153–1155. [[CrossRef](#)]
21. Ashkenani, H.; Taher, M.A. Use of Ionic Liquid in Simultaneous Microextraction Procedure for Determination of Gold and Silver by ETAAS. *Microchem. J.* **2012**, *103*, 185–190. [[CrossRef](#)]
22. Pallotta, A.; Philippe, V.; Boudier, A.; Leroy, P.; Clarot, I. Highly Sensitive and Simple Liquid Chromatography Assay with Ion-Pairing Extraction and Visible Detection for Quantification of Gold from Nanoparticles. *Talanta* **2018**, *179*, 307–311. [[CrossRef](#)]
23. Lopez-Chaves, C.; Soto-Alvaredo, J.; Montes-Bayon, M.; Bettmer, J.; Llopis, J.; Sanchez-Gonzalez, C. Gold Nanoparticles: Distribution, Bioaccumulation and Toxicity. In Vitro and in Vivo Studies. *Nanomed. Nanotechnol. Biol. Med.* **2018**, *14*, 1–12. [[CrossRef](#)] [[PubMed](#)]
24. Tournebize, J.; Boudier, A.; Joubert, O.; Eidi, H.; Bartosz, G.; Maincent, P.; Leroy, P.; Sapin-Minet, A. Impact of Gold Nanoparticle Coating on Redox Homeostasis. *Int. J. Pharm.* **2012**, *438*, 107–116. [[CrossRef](#)]
25. Pallotta, A.; Boudier, A.; Leroy, P.; Clarot, I. Characterization and Stability of Gold Nanoparticles Depending on Their Surface Chemistry: Contribution of Capillary Zone Electrophoresis to a Quality Control. *J. Chromatogr. A* **2016**, *1461*, 179–184. [[CrossRef](#)] [[PubMed](#)]
26. Pallotta, A.; Boudier, A.; Creusot, B.; Brun, E.; Sicard-Roselli, C.; Bazzi, R.; Roux, S.; Clarot, I. Quality Control of Gold Nanoparticles as Pharmaceutical Ingredients. *Int. J. Pharm.* **2019**, *569*, 118583. [[CrossRef](#)]
27. ICH. Q2(R1) Note for Guidance on Validation of Analytical Procedures: Text and Methodology Ref. CPMP/ICH/381/95. Available online: <https://ich.org/page/quality-guidelines> (accessed on 16 March 2021).
28. Food and Drug Administration. *Guidance for Industry, Bioanalytical Method Validation*; U.S. Food and Drug Administration: Silver Spring, MD, USA, 2018.
29. Akinyele, I.O.; Shokunbi, O.S. Comparative Analysis of Dry Ashing and Wet Digestion Methods for the Determination of Trace and Heavy Metals in Food Samples. *Food Chem.* **2015**, *173*, 682–684. [[CrossRef](#)]

30. Sonavane, G.; Tomoda, K.; Makino, K. Biodistribution of Colloidal Gold Nanoparticles after Intravenous Administration: Effect of Particle Size. *Colloids Surf. B Biointerfaces* **2008**, *66*, 274–280. [[CrossRef](#)]
31. Yang, L.; Kuang, H.; Zhang, W.; Aguilar, Z.P.; Wei, H.; Xu, H. Comparisons of the Biodistribution and Toxicological Examinations after Repeated Intravenous Administration of Silver and Gold Nanoparticles in Mice. *Sci. Rep.* **2017**, *7*, 3303. [[CrossRef](#)] [[PubMed](#)]
32. Lasagna-Reeves, C.; Gonzalez-Romero, D.; Barria, M.A.; Olmedo, I.; Clos, A.; Sadagopa Ramanujam, V.M.; Urayama, A.; Vergara, L.; Kogan, M.J.; Soto, C. Bioaccumulation and Toxicity of Gold Nanoparticles after Repeated Administration in Mice. *Biochem. Biophys. Res. Commun.* **2010**, *393*, 649–655. [[CrossRef](#)]
33. Pallotta, A.; Clarot, I.; Sobociński, J.; Fattal, E.; Boudier, A. Nanotechnologies for Medical Devices: Potentialities and Risks. *ACS Appl. Bio Mater.* **2018**, *2*, 1–13. [[CrossRef](#)]